RASĀYAN *J. Chem.*
Vol. 17 | No. 2 |391-403| April - June | 2024
ISSN: 0974-1496 | e-ISSN: 0976-0083 | CODEN: RJCABP
http://www.rasayanjournal.com
http://www.rasayanjournal.co.in

NATURAL CLAY MINERALS FOR REMOVAL OF CATIONIC DYE: KINETIC, ADSORPTION, AND THERMODYNAMIC STUDY

Shilpa Yakkerimath[1], Raviraj M. Kulkarni[1,3,✉], Sanjaykumar V. Divekar[1], Vaibhav R. Chate[2,3] and Purandara Bekal Kunkangar[2]

[1]Department of Chemistry, KLS Gogte Institute of Technology (Autonomous) affiliated to Visvesvaraya Technological University, Udyambag, Belagavi Karnataka-590008

[2]Department of Civil Engineering, KLS Gogte Institute of Technology (Autonomous) affiliated to Visvesvaraya Technological University, Udyambag, Belagavi Karnataka-590008

[3]Centre for Nanoscience and Nanotechnology, KLS Gogte Institute of Technology (Autonomous) affiliated to Visvesvaraya Technological University, Udyambag, Belagavi Karnataka-590008

✉Corresponding Author: ravirajmk@git.edu

ABSTRACT

In recent years managing ecological changes and comprehending diverse anthropogenic contributions towards pollution is now of great concern due to industrialization. Therefore, creating an environmentally friendly solution for dealing with harmful substances like Methylene Blue in water has become a critical issue. This experimental investigation aims to design and assess the unmodified clay mineral of the Panchaganga River flood zone for the removal of MB by batch tests. The removal of MB was examined by optimizing all the variables, further XRD, SEM, EDX, BET, and FTIR, were all used to meticulously examine the NC before and after adsorption. Methylene Blue content was determined by UV-visible spectrophotometrically, and the mechanism of NC's adsorption to MB in water was examined by modeling isotherm and kinetics studies. At pH 7.00 to 8.00, the NC showed a high extraction of MB due to negatively charged clay surface (Si-O^-), (Al-O^-). The adsorption capacity q_m obtained was 88.8 mg/g (Langmuir). The kinetics study showed that the adsorption mechanism follows pseudo-2nd-order indicating chemisorption as a rate-determining step, moreover, adsorption also occurs via the intra-particle-diffusion process due to small pores on NC. The study demonstrates that the NC exhibits significant efficacy in efficiently removing the cationic dye (MB) pollutant from waste-water systems.

Keywords: Methylene Blue Adsorption, Cationic Dye, Natural Clay, Chemisorption, Kinetic, Isotherm.

RASĀYAN *J. Chem.*, Vol. 17, No. 2, 2024

INTRODUCTION

In the evolving prerequisite of a growing population, and increased demand for essentials (food, water, clothing, etc.), to meet the requirements industrial growth has accelerated in recent decades in all sectors. This has led to a crisis in freshwater availability due to deterioration by a continuous discharge of industrial effluents to the nearby freshwater stream. The non-biodegradable pollutants like dyes entering the natural environment are of great concern.[1,2] The textile industries produce huge amounts of effluent containing colored moiety having complex aromatic structures and their degradation leads to carcinogenic, mutagenic products[3,4] 'Methylene blue' is a dark blue colored dye used in textile industries, also used as a biological stain, readily miscible in water causing harmful impacts on the aquatic environment. Hence, removing these organic dyes has emerged as a significant issue in past decades. Various methods have been devised to eradicate MB from polluted water,[5–7] especially biological methods, chemical (Fenton, ozonolysis)[8], biodegradation, membrane separation, electrochemical reactions[9], flocculation, and adsorption to eliminate MB from wastewater. The adsorption remedy is recognized as a remarkably effective procedure due to its advantages over all traditional techniques such as being cost-efficient, easy, and not adding toxic chemicals. This has attracted many scientists to work on adsorption processes utilizing various adsorbents to remove MB based on their properties. However, the lack of reusability and high cost of the adsorbents have

http://doi.org/10.31788/RJC.2024.1728772

overtaken many low-cost and highly efficient materials like agricultural wastes [10,11], industrial secondary products, biomass[12], and natural resources (clays and modified clays). [13–16] Numerous investigations on clays for adsorption of dyes have been reported. Clays are naturally available and abundant in environments with physicochemical properties like substantial surface area, capability for cation exchange (CEC), and electronegativity making them more effective in eliminating hazardous pollutants. Moreover, these clay minerals differ in their properties, and structures (octahedral- Al^{3+}, Fe^{3+}, Fe^{2+}, Mg^{2+}, and tetrahedral -Si^{4+}) depending on geography. Hence, many researchers are paying considerable attention to eco-friendly materials for pollution remediation

Therefore, the main focus of the research endeavor was not only to investigate whether the natural clay mineral obtained from the Panchganga river flood zone [17] is effective for the adsorption of MB but also for the type of sorption processes controlling the adsorption. This was achieved by conducting laboratory analysis using simulated methylene blue (MB) solution at different temperatures, pH, kinetics, and thermodynamics. However, the unmodified clay with a high percentage of silica, aluminum, and iron provides large surface groups for interaction with MB and has a high specific surface area with a mesoporous structure that provides voids for the dye adsorption making the natural clay an excellent adsorbent.

Materials and Batch Procedures

In the current investigation, the sediment samples (reddish brown lateritic soil) from the Panchganga river were collected from the locations 16º41´51´´North Latitude and 74º 9´59.4´´East Longitude (Fig.-1) and used as adsorbent. Methylene blue (Sigma Aldrich) was used to prepare simulated dye effluent and analytical grade compounds were utilized in the investigation.

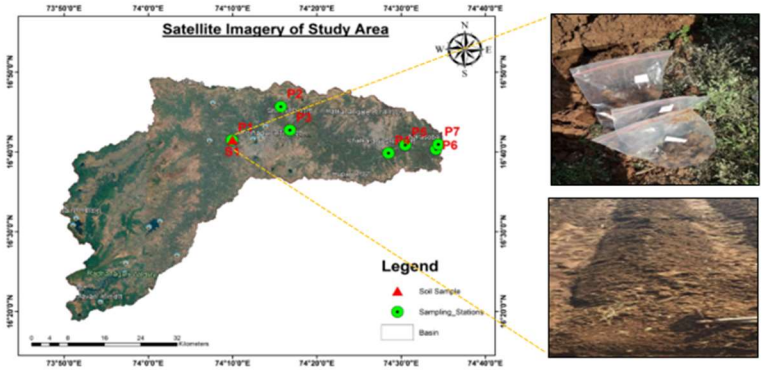

Fig.-1: Location of NC Sample from Flood Zone of Panchagnaga River

A batch adsorption experiment was conducted with 100 cm^3 of MB solution, NC (0.02 g) in 200 mL bottles wrapped with Al foil to prevent exposure to light. The bottles were kept for agitation in the "water bath shaker" (Toshiba Make Thermostat) for 2 hrs. at temperatures 298, 303, and 318 K, until equilibrium was reached and agitated at 1200 rotation speed for 10 min. The amount of MB in the aliquot was determined using a UV-visible spectrophotometer (Agilent Cary 60 USA) calibrated to 664 nm.

The quantity of adsorption at equilibrium, q_e (mg/g) estimated by:

$$q_e = \frac{(Co- \quad)xV}{W} \tag{1}$$

Where, C_o - initial concentration (mg/L), C_e - equilibrium concentration (mg/L), V - Volume of the solution, and, W - Weight of the adsorbent (g).

The adsorption (%) estimated by,

$$(\%\ R) = \left(\frac{C_o - C_a}{C_o}\right) x100 \tag{2}$$

Where, C_a is the concentration of adsorbate at any time (mg/L)

EXPERIMENTAL

Preparation of MB and NC

A predetermined quantity of MB is dissolved in Millipore water to obtain the stock solution., which is utilized to prepare the standard solution and the pH of the MB aliquot is set (HCl and NaOH solutions) for further analysis. Acquired sediment samples were finely pulverized in mortars, through a 75 μm screen, and then dried for 24 hours at 100 °C in a furnace.

Characterization (NC) Techniques

The mineral structures of the clay are analyzed utilizing XRD (Model: Smart Lab SE), employing monochromatic Cu-K irradiance (λ=154 nm) and a scan rate of 10^4 per min in the interval of 10-90º, was utilized to study the crystal structure of the clay sample. The Scherrer Eq 3 was used to calculate the clay's grain size.

$$Dp = \frac{k\lambda}{\beta co\ \theta} \quad (3)$$

Where Dp denotes the average size of the ordered crystalline, k denotes dimensionless shape constant 0.94, λ is X-ray wavelength 0.154 nm, β denotes the width of the line at half its maximum intensity (FWHM), and Θ denotes the Bragg angle. A SEM generates images on nano-micro scale resolution thus enabling a greater idea of the surface topography, orientation of minerals, and texture of the study material. To determine the surface morphology, a JSM-IT500 instrument equipped with an EDX detector for the elemental analysis at an accelerated voltage of 10kV with a spot size of 8.8mm was used to study the NC. An infrared spectroscope was used to investigate the NC (before and after adsorption) surface-functional group (Thermo-Scientific, Nicolet iZ10) in a wavelength (4000 and 400 cm^{-1}) at a magnification of 4 cm^{-1}. A N_2 sorption isotherm analysis was conducted using the 'BELSORP- Mini (II) (BEL Japan)' instrument to ascertain the surface area, pore volume, and pore size distribution. The adsorption/ desorption isotherms were measured after degassing the clay sample below 10^{-2} kPa at 200ºC for 4 hours at 77 K. According to the solid surface's ability to form a monolayer of N_2 gas molecules, the surface area is calculated., and the pore size and volume are ascertained by the capillary condensation method. A particle size analyzer was used to determine the 'Zeta potential' and 'particle size', (Horiba Scientific, SZ100Z Nano Particle Analyzer) to assess the stability and mean particle size of NC PMT experiment is utilized to estimate the NC's point of zero charges (PZC), described by Umer Farooq et al 2011.[18]

RESULTS AND DISCUSSION

NC Analysis

XRD spectrum (Fig.-2) depicts the crystal structure of the NC. Several diffraction peaks appeared in the pattern with 2Θ=20.914, 26.681, 40.346, 50.171, and 68.681 representing quartz with JCPDS No. 86-1628, 2Θ=21.376, 36.710 peaks are due to Cristobalite, corresponds to JCPDS No. 76-1390, Rutile 2Θ= 27.820, 54.186 with JCPDS No. 82-0514, Hematite at 2Θ= 32.631, 35.560, 53.236, with JCPDS No. 89-0598, and Al_2O_3 2Θ= 33.204, 75.740 with JCPDS No. 78-5510, the regions of 2Θ=32.63, 35.56 are attributed to the (104), (110) of α-Fe_2O_3.[19] The clay's grain size was estimated using Scherrer's equation. It was obtained from the calculation as 82.43nm, which closely matches the size measured by the particle size analyzer. (Fig.6b). Hence XRD results depict the NC mineral framework (SiO_2, Al_2O_3) and particle size of the crystals. SEM photographs depict the morphological characteristics of an NC particle, the magnification 7000 revealed two distinct types of microstructures. The first kind is depicted as lath-shaped, spherical pieces of crystallized 2:1 illite material[20], and the second form is quartz, which consists of almost dimensional particulates with smooth edges with rough surfaces.[21] Further images of magnification 3000 shown in Fig.-3a depict the surface with many pores that are diverse in size and shape, which offer a substantial quantity of active areas for the uptake of MB. The EDX spectra (Fig.-3c) show the presence of a high percentage of silica (8.72 %), iron (8.01%), and alumina (5.58%), which provide broad surface groups for interactions and cause the uptake of cationic MB responsible for the adsorption of organic dye by providing large surface groups for interactions. Various functional groups upon adsorbent were identified using FTIR analysis, and its impact on adsorption was further investigated. From Fig.-4 the IR absorption in the 1150–400 cm^{-1} range is attributable to lattice vibration and is also comparatively more instructive concerning structural features of clay minerals. A band at 752 cm^{-1} is attributed to water's O-H

stretching mode. The most prominent peaks in O-H asymmetric stretching are observed at 3402 cm^{-1}, physically adhered water molecules cause a peak to be seen at 1637 cm^{-1} further at 470.4 cm^{-1}, 534cm^{-1}, and 1033cm^{-1} silanol in-plane bending, symmetric stretching, asymmetric stretching vibration observed confirms the presence of quartz[22], peak at 752 cm^{-1}, 913 cm^{-1} are Al-OH bending, and band 534 cm^{-1} reflects the vibrations of Silicon-Oxygen-Aluminium bending. The vibration of O-Al-OH has been ascribed to a band at 655.8 cm^{-1}.[23] Furthermore, after the adsorption of MB, a shift in the characteristics band of clay was observed to a higher frequency of 1388 cm^{-1} to 1400 cm^{-1} due to the interaction of clay with MB. Still, significant enhancement at 1400 cm^{-1} was noticed, and this band is due to vibrations induced by MB's phenyl ring.[24] In addition, a new band appeared at 3128 cm^{-1} due to the C-H asymmetric stretching bond in the aromatic ring of MB. It was found that the intensities of all bands increased upon adsorption. Therefore, it confirms the uptake of MB. Surface properties of NC were assessed by analyzing N2 adsorption/desorption isotherms at 77K temperature, as shown in Fig-5. The resulting curve, which displays the mesoporous morphology of clay[25], also shows a type-IV isotherm with an "H4-type" hysteresis loop following the IUPAC classification. [26,27] The distribution of pore sizes determined by the BJH method in Fig.-5 reveals pores like small slits, which refers to the initial filling of MB on mesoporous occurs by adsorption on an external surface. According to the findings, clay has a large surface area of 78.253 (m^2. g^{-1}) and a mesoporous size of about 6.39 nm. Previous studies substantiate that there is an increase in specific areas of clay accordingly with heating temperature (100 to 300ºC) due to the removal of water from nano-porous chambers and also from coordinated water. From the zeta potential and particle sizer (Fig.-6), the clay particles estimated were around 82.6 nm in size, with 75.3 nm being the average size. The average zeta potential, derived from three measurements, was found to be -48 mV. The existence of a negative charge on NC's surface is indicated by the negative zeta potential. The PZC of NC was estimated by the PMT experiment and the obtained pH_{PZC} for NC was at pH 5.

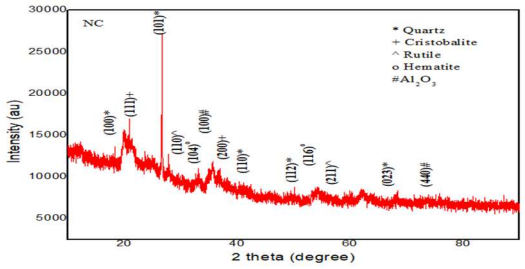

Fig.-2: XRD Pattern of NC

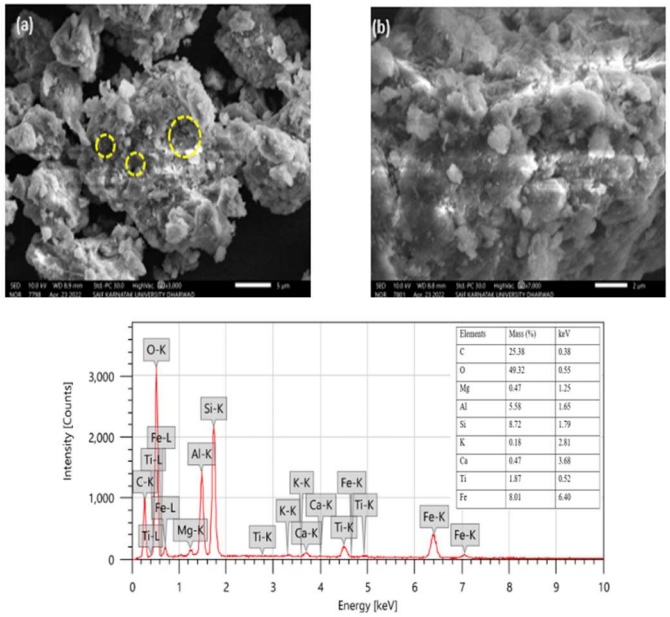

Fig.-3: (a) SEM Image of NC at x3000 Magnification (b) x 7000 Magnification (c) EDX Pattern of the NC

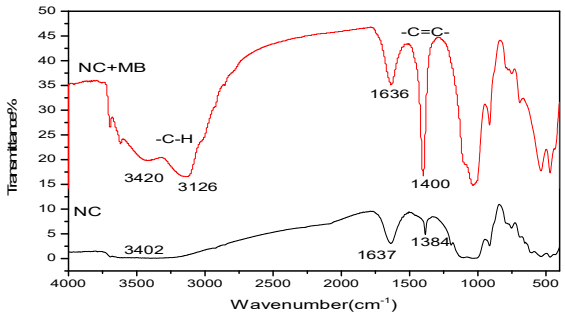

Fig.-4: FTIR Spectrum of NC, MB Loaded on NC

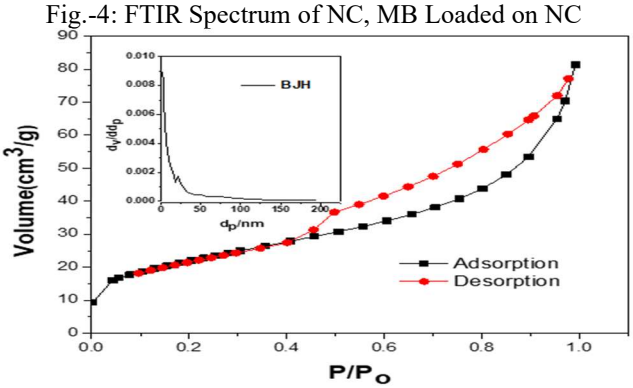

Fig.-5: NC's BJH Pore Size Distribution and N_2 Adsorption/Desorption Isotherm.

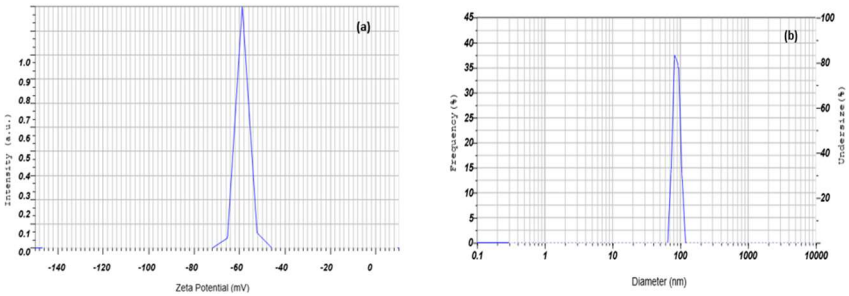

Fig.-6: (a) Zeta Potential and (b)Particle Size of NC

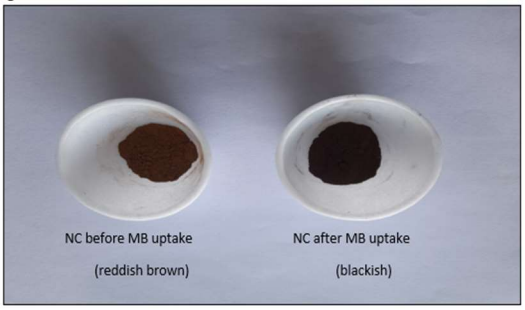

Fig.-7: Images of NC (before and after) Adsorption of MB

Effect of Interaction Time

The adsorption kinetics study of MB on NC at a dosage of 0.020 g, at a fixed strength of 100 ml MB solution was examined and the proportion of MB over each period was measured spectrophotometrically. The hydroxyl group on surfaces of clay promotes the adsorption of positively charged ions via electrostatic contact. The Fig.-8a illustrates a significant difference in MB removal over contact time. Initially adsorption of MB spikes with contact time, and achieves the maximum removal efficiency of 92.2% at 215 mins, suggesting monolayer accumulation of MB on the clay's surface, due to the greater count of empty sites available for binding. After 215 min the process reached an equilibrium stage, therefore, no significant vacant binding sites on the NC-adsorbent for further extraction. [28,29]

Influence of Different MB Concentrations

The aliquot's, MB concentration was adjusted between 3.73 to 22.43 mg/L and the impact of MB concentration on clay was examined. The uptake of MB by clay adsorbent is shown to be significantly influenced by concentration, as seen in Fig.-8b. It was noticed that when the aliquot's MB strength increased, the removal percentage decreased. The primary cause for the decrease at higher strength of MB is due to a reduction of available binding sites. [30]

Effect of NC Dose

MB's uptake was studied by increasing the quantity within 0.005 - 0.050 g by keeping other reaction parameters constant. The below Fig.-8c demonstrates the increased dosage amount directly raised the removal rate from 52.6 % to 96.4 %, this increase is driven by porosity with expanding contact regions as well as the availability of additional reactive adsorption sites.[31] Additionally, the figure shows that MB's adsorption was quickly increased to 0.020 g/L of dosage and the subsequent increase had not much impact on MB's removal. It's mainly because of achieving equilibrium between adsorbent and adsorbate. [32]

Effect of pH

The sorption of MB onto NC is influenced by the pH of the solution, which is in turn affected by the clay surface charges and the degree of dissociation of MB. In the current investigation, using buffering agents (acetate, phosphate, and borate) the pH of the MB aliquot was changed while maintaining other variables constant. The findings from Fig.-8d indicate that within the pH range of 7.0 to 8.0, the optimal removal factor (%R) was 90.2% and it accounted for electrostatic interaction. At higher pH, H^+ ion concentration in the aliquot is dropped hence no competing ions with MB for adsorption on NC, and pH_{PZC} of clay was obtained at pH 5 by PMT experiment, therefore the highest uptake of cationic MB was favored at higher pH due to negatively charged clay surface ($Si\text{-}O^-$), ($Al\text{-}O^-$) [33,34]. However, at pH< $pH_{PZC,}$ the positively charged clay's surface ($Si\text{-}OH_2^+$) and ($Al\text{-}OH_2^+$) create electrostatic repulsion, and hence less removal factor(%R) was obtained. Hydrogen bonds, n-π interactions, and electrostatic attraction cause MB to bind clay material. Since clay has hydroxyl sites at the surface that are called aluminol (Al-OH) and silanol (Si-OH), they provide a negative surface of clay (pH>5) forming electrostatic interaction with the nitrogen of MB[35]. However, silanol and aluminol groups form hydrogen bonds with an amine group of MB, and also MB cations undergo ion exchange with the Ca^{2+} and Mg^{2+} of clay minerals. Along with these interactions, the electron cloud of the benzene ring in MB and the oxygen lone pair electrons are found to interact via the n-π interaction (Fig.-9).

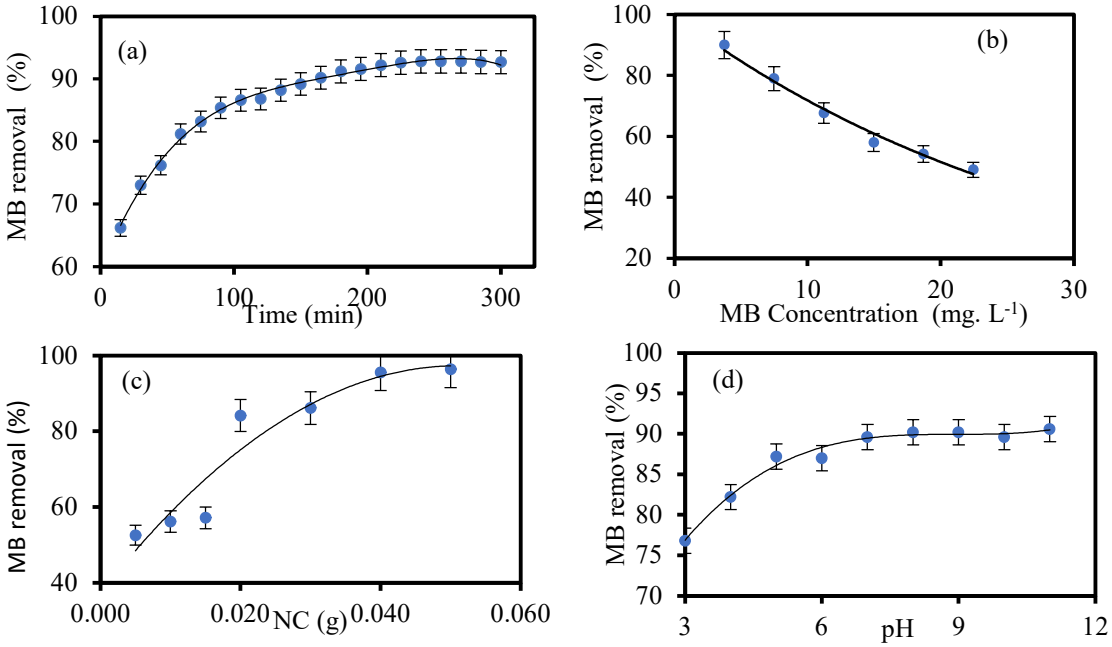

Fig.-8: Effect of (a) Interaction Time (b) MB Concentration (c) NC Dose (d) pH

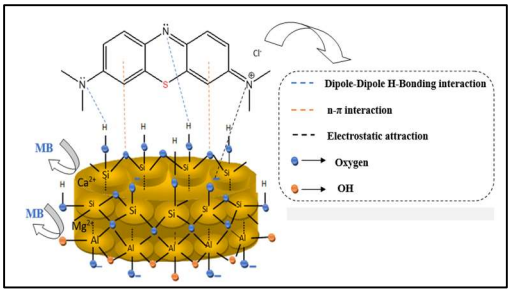

Fig.-9: Plausible Mechanism for Sorption of MB on NC

Isotherm Modeling Study

Langmuir, Freundlich, and Redlich-Peterson isotherms were utilized in the experiment to analyze the equilibrium outcomes of the MB adsorption on the NC

The Langmuir - isotherm equation is [36,37]:

$$\frac{C_e}{q_e} = \frac{C_e}{q_m} + \frac{1}{K_L q_m} \quad (4)$$

Figure-10a shows a linear plot, where K_L and q_m signify Langmuir constant (L/g) and adsorption energy (mg. g^{-1}), C_e represents the aliquot's MB concentration at equilibrium (mg/L), q_e is adsorption capacity at equilibrium (mg/g). The isotherm shows that the uniform one-layer adsorption has precisely the same activation energy. The separation factor R_L suggests the nature of the adsorption is unfavorable (R_L>1), linear (R_L=1), and irreversible (R_L=0) [38].

$$R = \frac{1}{1+K_L C_0} \quad (5)$$

The results of calculated values suggest that the sorption of MB on NC is favorable (0<R_L<1), and also the R^2 values for all temperatures were higher indicating the equilibrium data matches well with the Langmuir-isotherm. The findings of the isotherms are presented in Table-1.

The straight-line equation illustrates a heterogeneous surface energy system with multilayer adsorption and the model equation is [39],

$$\log q_e = \log K_f + \frac{1}{n_f} \log C_e \quad (6)$$

Therefore, the adsorption potential at equilibrium is denoted by qe, K_f, and n_f are the isotherm constant that depicts the adsorption capacity and strength. The consistent values K_f and n_f are derived from the $\log q_e$ vs. $\log C_e$ graph below. Table-1 shows that the n_f values were all above 1, suggesting adsorption is effective. Moreover, a temperature-dependent increase in K_f values further supports the adsorption's endothermic nature.

A hybrid model of the Langmuir and Freundlich is the RP isotherm. The model's linear equation is [40],

$$q_e = \frac{A_r C_e}{1+BC_e^{\beta}} \quad (7)$$

A_r in the equation signifies the RP isotherm constant, and the exponent with a value in the range of 0 to 1 is represented by β. From the above Eq (7), the RP model simplifies to the Langmuir model as β gets closer to unity. Likewise, when C_e gets closer to infinity, RP decreases to the Freundlich. From the finding in Table-1, the β value is close to unity indicating adsorption follows Langmuir, moreover, the Freundlich model's coefficient (R^2) is significantly lower than that of the Langmuir and RP models, suggesting that monolayer chemisorption is the primary mechanism involved in the uptake of MB on NC. [41]

Adsorption Kinetics

The kinetic analysis demonstrates the impact of the interaction period on the rate of MB sorption on NC. It is studied by taking a 100 cm^3 solution of a specified concentration with 0.02 g of NC. The amount of MB that remained upon adsorption was recorded using spectrophotometric analysis. Experimental results were examined for adsorption response models such as pseudo1st-order, pseudo-2nd-order, Ritchie 's-2nd-order, and intra-particle diffusion.

The pseudo-1st-order kinetics predicts the quantity of accessible interaction spots on the adsorbents is positively correlated with the rate of adsorption. [42]

$$\log(q_e - q_t) = \log q_e - \left(\frac{k_1}{2.303}\right) t \quad (8)$$

where, q_t is the volume of MB that was absorbed at the moment (t) in (mg. g^{-1}), q_e –is the amount of MB deposition per mass of clay at equilibrium, and k_1 denotes rate constant (min^{-1}). k_1 and q_e are estimated using the intercept and slopes of the curve shown in below Fig.-11a of log (q_e-q_t) vs. t (min).

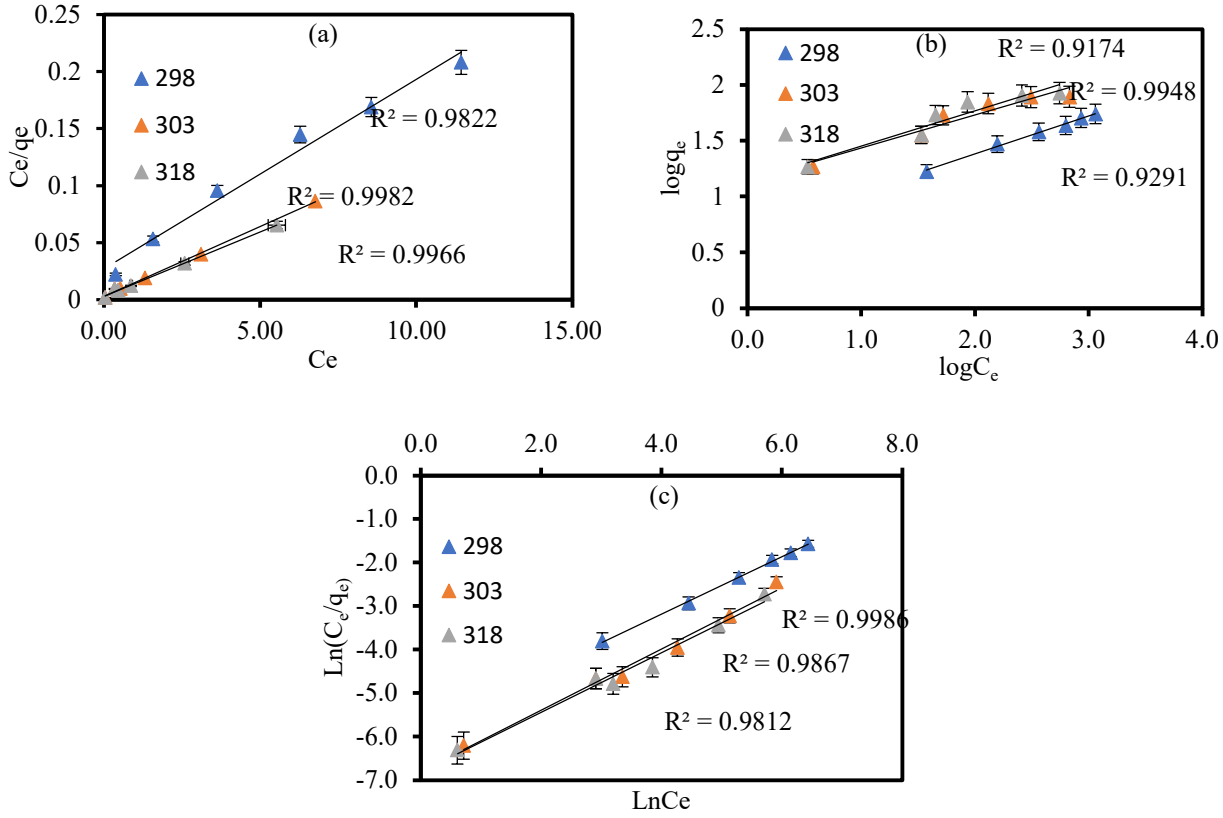

Fig.-10: (a) Langmuir (b) Freundlich (c) Redlich-Peterson Isotherms for MB Adsorption on NC at (298, 303, and 318 K).

Table-1: Adsorption of MB onto NC: Isotherm Parameters

S.No.	Isotherm Model	Isotherm parameters	Temperature (K)		
			298	303	318
1	Langmuir	K_L(L/g)	0.604	3.879	3.531
		q_m(mg/g)	60.289	81.764	88.886
		R_L	0.237	0.113	0.147
		R^2	0.982	0.998	0.996
2	Freundlich	n_f	2.939	3.374	3.170
		K_f (L/mg)	5.040	13.759	13.739
		R^2	0.994	0.929	0.917
3	Redlich –Peterson	β	0.660	0.704	0.685
		Ar(L/g)	338.102	898.804	907.910
		R2	0.998	0.990	0.981

Table-2, shows relative model parameters and demonstrates a discrepancy between the value computed for qe and those found experimentally, therefore, the adsorption mechanism is not entirely close to pseudo-1st-order kinetics (Fig.-11a) but deviated after a short interval of time.

The pseudo-2nd-order kinetics depicts a phase of adsorption that is limited by the rate of chemisorption. The expression for the kinetic model is given as: [43,]

$$\frac{t}{q_t} = \frac{1}{k_2 q_e^2} - \frac{1}{q_e} t \quad (9)$$

k_2 denotes the rate constant, (g $mg^{-1}min^{-1}$), and the values of k_2 and q_e can be derived by analyzing the slope and intercept of the t/q_t vs t (min) plot, subsequently given in the below Fig.-11b. The model yields an R^2 value that is significantly larger than 1st-order, and both computed and empirically obtained qe values agree well, indicating that pseudo-2nd-order kinetics govern the adsorption of MB on NC, signifying chemisorption to be the rate-determining phase [44]. The finding of the kinetics is summarized in Table-2.
The Ritchie's- 2nd-order kinetic model that derives the adsorbent as energetically homogenous is represented in Eq. (10). [45]

$$\frac{1}{q_t} = \frac{1}{k_r q_e t} + \frac{1}{q_e} \quad (10)$$

q_e (mg g-1) and k_r (1/min) are estimated from the intercept and slope of a line graph $1/q_t$ vs. 1/t (min-1), respectively. The data shown in Table-2 indicate that Ritchie's 2nd-order model exhibits a high R^2 value of 0.9913, suggesting a strong fit between the adsorption process and this model.
The IPD model provides a thorough explanation of the adsorption process since the adsorption is controlled by diffusion. It identifies the rate-determining phase involved in the sorption process. Expression of IPD is [46],

$$q_t = k_{ipd} t^{\frac{1}{2}} + A \quad (11)$$

q_t is the quantity of MB absorbed in time 'mg/g', k_{ipd} is a measure of the IPD coefficient mg/g. $min^{1/2}$, and A denotes constant referring to the barrier layer's thickness. However, the slope of the q_t (m) against the $t^{1/2}$ (min) plot depicts the k_{ipd} value. The below Fig.-11d shows multi-linearity curves not passing through the origin, as the first step- a sloped portion indicates high mass diffusion, however rate-determining step, IPD, is represented by the second linear portion, and subsequently the saturation phase in the third step.[47] According to Table-2's results, the adsorption of MB also proceeds by multiple steps, initially the adsorption of MB follows a surface diffusion, and then adsorption occurs through intra-particle diffusion.[48,49]

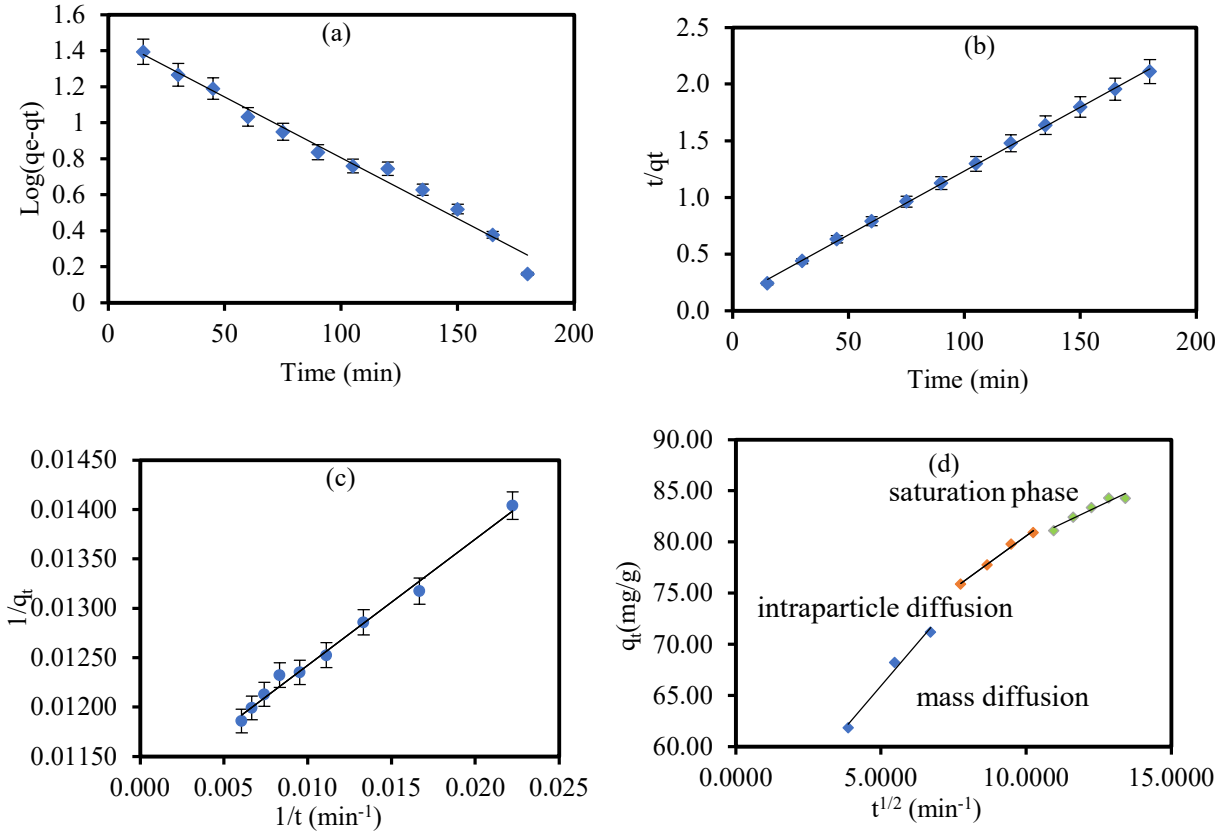

Fig.-11: Adsorption Kinetics (a) Pseudo-1st -Order (b) Pseudo-2nd -Order (c) 'Ritchie's- 2nd -Order' (d) 'IPD'

Table-2: Kinetic Factors of MB Removal by using NC

Adsorption Reaction Model	Factors	NC
Pseudo-1st -order	$k_1(min^{-1})$	0.015
	$q_e(mg/g)$	30.222
	R^2	0.981
Pseudo-2nd – order	$k_2(min^{-1})$	0.001
	$q_e(mg/g)$	88.756
	R^2	0.999
Ritchie's-2nd -order	$k_r(min^{-1})$	1160.92
	$q_e(mg/g)$	85.350
	R^2	0.991
IPD	k_{ipd} (mg. g^{-1}. $min^{1/2}$)	2.320
	A	56.10

Adsorption Thermodynamics

Thermodynamics study gives insight into the evaluation of the mechanisms of the adsorption approach. As the sorption is temperature dependent, therefore it is studied at different temperatures 298, 303, 318 K, and the parameters of thermodynamics (ΔH^o, ΔS^o, ΔG^o, and Ea). are determined through the use of equations (12) (13) (14) and (15)

$$\Delta G^0 = \Delta H^0 - T\Delta S^0 \quad (12)$$

$$\mathrm{In}K_c = \frac{\Delta S^0}{R} - \frac{\Delta H^0}{RT} \quad (13)$$

$$\Delta G^0 = -RT\mathrm{ln}K_D \quad (14)$$

$$lnk_c = \mathrm{ln}A_a - \frac{E_a}{RT} \quad (15)$$

R and Kc stand for the equilibrium constant and natural gas's constant, respectively. Gibbs free energy ΔG^0 value is estimated from Eq (14), further enthalpy (ΔH^o), entropy (ΔS^o) is derived by slope and intercept of a chart $\ln K_c$ vs 1/T using linear Eq (13). A_a and E_a are frequency factors and activation energy[50], the values are obtained from the below plot. According to Table-3 adsorption is spontaneous, as shown by the negative ΔG^o values, however, the endothermic phenomenon is demonstrated by the positive ΔH^o value, positive ΔS^o value indicates randomness after the adsorption of MB on NC at solid-aqueous medium interface.[51] The E_a value obtained for the MB adsorption on NC was 92.83 'kJ/mol' indicating chemical sorption as the rate-limiting phase.[52] Table-3 illustrates a rising trend in MB adsorption on NC as temperature is increased because higher temperatures create more open sites for adsorption, enhancing intra-particle-diffusion.

Table-3: Thermodynamic Variables for MB (dye) Adsorption on NC

Temperature (K)	ln k_c	ΔG^o kJ. mol^{-1}	ΔH^o 'kJ. mol^{-1}	ΔS^o 'J. $(mol\ K)^{-1}$	E_a kJ. mol^{-1}	A_a
298	2.91	-6.945	92.831	0.334	92.83	$3.089x10^{17}$
303	3.27	-8.619				
318	5.20	-13.641				

CONCLUSION

Natural clays found in the Panchganga River show good adsorption efficiency for MB. Additionally, it was revealed that 0.02 g at 7.0 pH was the ideal amount for MB adsorption on NC. To comprehend the adsorption phenomenon, isotherm investigations were conducted and the results of isotherm analysis revealed that the Langmuir model has the highest correlations (R^2) for MB adsorption onto NC which indicates the adsorption occurs through chemisorption as a major process. In comparison to the pseudo-1st-order kinetics, the results of pseudo-2nd order and Ritchie 's-2nd-order represent the best correlations with experimentally and calculated qe value. Therefore rate-controlling stage of MB adsorption on NC initially occurs through chemisorption mechanisms. According to the thermodynamic variables ΔG^o, ΔH^o, and ΔS^o, a negative ΔG^o strongly suggests the process is favorable and spontaneous, a positive Enthalpy change (ΔH^o), reveals the process is endothermic, and a positive Entropy change (ΔS^o), confirms adsorption as stable and categorized by clay's affinity for MB. The current study results showed that MB is largely removed from the modeled water system by the NC of the Panchganga River flood zone.

ACKNOWLEDGEMENTS
The authors are highly grateful to the authorities of their institutes.

CONFLICT OF INTERESTS
The authors declare that there is no competing interest.

AUTHOR CONTRIBUTIONS
All the authors contributed significantly to this manuscript, participated in reviewing/editing and approved the final draft for publication. The research profile of the authors can be verified from their ORCID ids, given below:

Shilpa Yakkerimath http://orchid.org/0009-0000-7481-9287
Raviraj M. Kulkarni http://orchid.org/0000-0001-6894-6888
Sanjaykumar V. Divekar https://orchid.org/0000-0002-5077-1992
Vaibhav R. Chate http://orchid.org/0000-0002-8562-6250
Purandara Bekal Kunkangar http://orchid.org/0000-0001-6863-2248

REFERENCES
1. N. Aryal, J. Wood, I. Rijal, D. Deng, M. K. Jha, A. Ofori-Boadu, *Water Environment Research,* **92(10)**, 1587(2020), https://doi.org/10.1002/wer.1404
2. G. Samchetshabam, T. G. Choudhury, S. Gita, *Environment & Ecology*, **3C**, 2349(2017).
3. T. Robinson, G. Mcmullan, R. Marchant, P. Nigam. *Bioresource Technology,* **77**,247(2001).
4. S. H. Siddiqui, M. K. Uddin, R. Isaac, O. F. Aldosari, *Adsorption Science and Technology,* 1-13 (2022).
5. R. Wibulswas, *Separation and Purification Technology*, **39**,3(2004).
6. S. P. Kim, H. C. Choi, *Bulletin of the Korean Chemical Society,* **35(9)**, 2660(2014), https://doi.org/10.5012/bkcs.2014.35.9.2660
7. J. Liu, S. Zuo, L. Yu, Y. Yu, B. Li, P. Chen, *Particuology,* **11(6)**,728(2013), https://doi.org/10.1016/j.partic.2013.01.006
8. Z. Wu, W. Zhu, M. Zhang, Y. Lin, N. Xu, F. Chen, D. Wang, Z. Chen, *Industrial & Engineering Chemistry Research,* **57(16),** 5539(2018), https://doi.org/10.1021/acs.iecr.8b00077
9. C. Comninellis, A. Kapalka, S. Malato, S. A. Parsons, I. Poulios, D. Mantzavinos, *Journal of Chemical Technology & Biotechnology,* **83(6)**, 769(2008), https://doi.org/10.1002/jctb.1873
10. L. T. M. Thy, N. T. C. Linh, N. T. T. Tram, T. H. Tu, L. T. Tai, P. T. Khang, H. M. Nam, N. H. Hieu, M. T. Phong, *Journal of Nanomaterials,* **2021**, Article ID 4636531(2021), https://doi.org/10.1155/2021/4636531
11. H. Li, V. L. Budarin, J. H. Clark, M. North, X. Wu, *Journal of Hazard Materials,* **436**, 129174(2022), https://doi.org/10.1016/j.jhazmat.2022.129174
12. N. H. Solangi, J. Kumar, S. A. Mazari, S. Ahmed, N. Fatima, N. M. Mubarak, *Journal of Hazard Materials,* **416**, 125848(2021), https://doi.org/10.1016/j.jhazmat.2021.125848
13. Mohamed El-Habacha, Abdelkader Dabagh, Salek Lagdali, Youssef Miyah, Guellaa Mahmoudy, Fouad Sinan, Mohamed Chiban, Soulaiman Iaich and Mohamed Zerbet, *Environmental Science and Pollution,* (2023), https://doi.org/10.1007/s11356-023-27413-3
14. V. K. Yadav, N. Choudhary, D. Ali, G. Kumar, G. Gnanamoorthy, A. U. Khan, P. Kumar, S. Hari Kumar, B. Z. Tizazu, *Adsorption Science & Technology,***2022**, 1-10, (2022), https://doi.org/10.1155/2022/8565151
15. H. H. Abdel Ghafar, E. K. Radwan, S. T. El-Wakeel, *ACS Omega,* **5(12)**, 6834(2020), https://doi.org/10.1021/acsomega.0c00166
16. T. Jiang, W. Zhang, A. K. Ilango, J. I. Feldblyum, Z. Wei, H. Efstathiadis, M. V. Yigit, Y. Liang, *ACS Applied Engineering Materials,* **1(1)**, 394(2023), https://doi.org/10.1021/acsaenm.2c00096

17. A. R. Kulkarni, *Pollution Resources,* **39(2)**, 437(2020).
18. U. Farooq, M. T. Tweheyo, J. Sjöblom, G. Oye, *Journal of Dispersion Science Technology,* **32(4)**, 519(2011), https://doi.org/10.1080/01932691003756936
19. U. Saidu, *Chemical Search Journal,* **10(2)**, 104(2019).
20. A. Islam, Z. Khan, M. Hussain, M. Uddin, *Dhaka University Journal of Biological Sciences,* **31(1)**, 105(2022), https://doi.org/10.3329/dujbs.v31i1.57920
21. A. Amar, I. Loulidi, A. Kali, F. Boukhlifi, C. Hadey, M. Jabri, *Applied and Environmental Soil Science,***2021**, Article ID 8826063(2021), https://doi.org/10.1155/2021/8826063
22. E. A. Ashour, M. A. Tony, *SN Applied Science,***2**, 2042(2020), https://doi.org/10.1007/s42452-020-03873-x
23. O. Meziane, A. Bensedira, M. Guessoum, N. Haddaoui, *Journal of Materials and Environmental Sciences,* **8(10)**, 3625(2017).
24. N. S. Randhawa, N. N. Das, R. K. Jana, *Desalination and Water Treatment,* **52(22-24)**, 4197(2014), https://doi.org/10.1080/19443994.2013.801324
25. A. H. Jawad, A. S. Abdulhameed, *Surfaces and Interfaces,***18**, 100422(2020), https://doi.org/10.1016/j.surfin.2019.100422
26. A. Mahandrimanana, *International Journal of Materials and Chemistry,* 1-4 (2020), https://doi.org/10.5923/J.IJMC.20201001.01
27. H. Chen, J. Zhao, A. Zhong, Y. Jin, *Chemical Engineering Journal,* **174(1)**, 143(2011), https://doi.org/10.1016/j.cej.2011.08.062
28. A. Gurses, C. Dogar, M. Yalcin, M. Acikyildiz, R. Bayrak, S. Karaca, *Journal of Hazardous Materials,* **131(1-3)**, 217(2006), https://doi.org/10.1016/j.jhazmat.2005.09.036
29. L. Lian, L. Guo, C. Guo, *Journal of Hazardous Materials,* **16(1)**, 126(2009), https://doi.org/10.1016/j.jhazmat.2008.03.063
30. B. Zohra, K. Aicha, S. Fatima, B. Nourredine, D. Zoubir, *Chemical Engineering Journal,* **136(2-3)**, 295(2008), https://doi.org/10.1016/j.cej.2007.03.086
31. A. Khenifi, Z. Bouberka, F. Sekrane, M. Kameche, Z. Derriche, *Adsorption,* **13(2),** 149(2007), https://doi.org/10.1007/s10450-007-9016-6
32. P. Senthil Kumar, M. Palaniyappan, M. Priyadharshini, A. M. Vignesh, A. Thanjiappan, P. Sebastina Anne Fernando, R. Tanvir Ahmed, R. Srinath, *Environmental Progress & Sustainable Energy,* **33(1)**, 87(2014), https://doi.org/10.1002/ep.11756
33. J. J. Salazar-Rabago, R. Leyva-Ramos, J. Rivera-Utrilla, R. Ocampo-Perez, F. J. Cerino-Cordova, *Sustainable Environment Research,* **27(1)**, 32(2017), https://doi.org/10.1016/j.serj.2016.11.009
34. R. Elmoubarki, F. Z. Mahjoubi, H. Tounsadi, J. Moustadraf, M. Abdennouri, A. Zouhri, A. El Albani, N. Barka, *Water Resources and Industry,* **9**, 16(2015), https://doi.org/10.1016/j.wri.2014.11.001
35. X. Tang, G. Ran, J. Li, Z. Zhang, C. Xiang, *Journal of Hazard Materials,* **402**, 123579(2021), https://doi.org/10.1016/j.jhazmat.2020.123579
36. E. Bulut, M. Özacar, İ. A. Şengil, *Microporous and Mesoporous Materials,* **115(3)**, 234(2008), https://doi.org/10.1016/j.micromeso.2008.01.039
37. O. Hamdaoui, *Journal of Hazardous Materials,* **135(1-3)**, 264(2005), https://doi.org/10.1016/j.jhazmat.2005.11.062
38. D. M. Salh, B. K. Aziz, S. Kaufhold, *Silicon,* **12(1)**, 87(2020), https://doi.org/10.1007/s12633-019-00100-0
39. H. K. Boparai, M. Joseph, D. M. O'Carroll, *Journal of Hazard Materials,* **186(1)**,458(2011), https://doi.org/10.1016/j.jhazmat.2010.11.029
40. L. S. Chan, W. H. Cheung, S. J. Allen, G. McKay, *Chinese Journal of Chemical Engineering,* **20(3)**, 535(2012), https://doi.org/10.1016/S1004-9541(11)60216-4
41. S. Chakrabarti, B. Chaudhuri, B. K. Dutta, *International Journal of Environment and Pollution,* **34(1/2/3/4)**,261(2008), https://doi.org/10.1504/IJEP.2008.020796
42. H. Qiu, L. Lv, B. Pan, Q. Zhang, W. Zhang, Q. Zhang, *Journal of Zhejiang University-SCIENCE A,* **10(5)**, 716(2009), https://doi.org/10.1631/jzus. A0820524

43. T. S. Kazeem, S. A. Lateef, S. A. Ganiyu, M. Qamaruddin, A. Tanimu, K. O. Sulaiman, S. M. Sajid Jillani, K. Alhooshani, *Journal of Cleaner Production,* **205**, 303(2018), https://doi.org/10.1016/j.jclepro.2018.09.114
44. B. K. Aziz, D. M. S. Shwan, S. Kaufhold, *Silicon,* **14(3)**, 893(2022), https://doi.org/10.1007/s12633-020-00833-3
45. E. Kakı, N. Gögsu, A. Altındal, B. Salih, Ö. Bekaroğlu, *Journal of Porphyrins Phthalocyanines,* **23**, 166(2019), https://doi.org/10.1142/S1088424619500196
46. W. J. Weber, J. C. Morris, *Journal of the Sanitary Engineering Division,* **89(2)**, 31(1963), https://doi.org/10.1061/JSEDAI.0000430
47. S. Ghorai, A. Sarkar, M. Raoufi, A. B. Panda, H. Schönherr, S. Pal, *ACS Applied Materials & Interfaces,* **6(7)**, 4766(2014), https://doi.org/10.1021/am4055657
48. M. N. Sahmoune, N. Ouazene, *Environmental Progress Sustainable Energy,* **31(4)**, 597(2012), https://doi.org/10.1002/ep.10594
49. H. Imam Maarof, N. Aida Zubir, N. Nasuha, H. Zurainan, H. Maarof, N. Zubir, N. Amri, *International Conference on Environmental Science and Engineering*, IPCBEE, Singapore, **8**, 51(2011).
50. M. A. Al-Ghouti, R. S. Al-Absi, *Scientific Reports,* **10(1)**, 15928(2020), https://doi.org/10.1038/s41598-020-72996-3
51. A. Özer, M. Toprak, *Environmental Progress Sustainable Energy,* **42(5)**, e14127(2023), https://doi.org/10.1002/ep.14127
52. X. S. Wang, Y. P. Tang, S. R. Tao, *Chemical Engineering Journal,* **148(2-3)**, 217(2009), https://doi.org/10.1016/j.cej.2008.08.020

[RJC- 8772/2024]